Turbulent drag reduction in nonionic surfactant solutions

Shinji Tamano,[1,a)] Motoyuki Itoh,[2] Katsuo Kato,[3] and Kazuhiko Yokota[1]
[1]*Graduate School of Engineering, Nagoya Institute of Technology, Gokiso-cho, Showa-ku, Nagoya, Aichi 466-8555, Japan*
[2]*Department of Mechanical Systems Engineering, Aichi University of Technology, 50-2 Manori, Nishihasama-cho, Gamagori, Aichi 443-0047, Japan*
[3]*JATCO Ltd., 700-1, Imaizumi, Fuji, Shizuoka 417-8585, Japan*

(Received 25 September 2009; accepted 4 March 2010; published online 4 May 2010)

There are only a few studies on the drag-reducing effect of nonionic surfactant solutions which are nontoxic and biodegradable, while many investigations of cationic surfactant solutions have been performed so far. First, the drag-reducing effects of a nonionic surfactant (AROMOX), which mainly consisted of oleyldimethylamineoxide, was investigated by measuring the pressure drop in the pipe flow at solvent Reynolds numbers Re between 1000 and 60 000. Second, we investigated the drag-reducing effect of a nonionic surfactant on the turbulent boundary layer at momentum-thickness Reynolds numbers Re_θ from 443 to 814 using two-component laser-Doppler velocimetry and particle image velocimetry systems. At the temperature of nonionic surfactant solutions, $T=25$ °C, the maximum drag reduction ratio for AROMOX 500 ppm was about 50%, in the boundary layer flow, although the drag reduction ratio was larger than 60% in pipe flow. Turbulence statistics and structures for AROMOX 500 ppm showed the behavior of typical drag-reducing flow such as suppression of turbulence and modification of near-wall vortices, but they were different from those of drag-reducing cationic surfactant solutions, in which bilayered structures of the fluctuating velocity vectors were observed in high activity. © *2010 American Institute of Physics*. [doi:10.1063/1.3407666]

I. INTRODUCTION

Surfactants are categorized into four types, namely, anionic, cationic, nonionic, and zwitterionic.[1] Among them, the cationic surfactant has been widely investigated as drag-reducing additives for wall-bounded turbulent flows, since it has high drag-reducing ability of up to 80%.[1–3] Recently, cationic surfactant has been practically utilized for a circulatory system, since such surfactants were little affected by the degradation due to mechanical shear action, so that they could be used for a long time without special treatment. However, a cationic surfactant does not degrade naturally due to bacteria, so the potential damage to the environment is much higher than with nonionic surfactants. So far, therefore, cationic surfactants have been applicable to only the closed loop system as drag-reducing additives.

On the other hand, a nonionic surfactant is nontoxic and biodegradable, and the potential damage to the environment is much smaller than that of a cationic surfactant, although, until recent developments, the drag-reducing ability of nonionic surfactant was not so high (typically less than 60%). Since the pioneering study of Zakin *et al.*[4,5] on the drag-reducing ability of nonionic surfactants, related studies have been reported for over 30 years. As pointed out in the review of Zakin,[1] nonionic surfactant molecules do not carry charges and thus they are less negatively affected by other ions such as calcium and magnesium ions normally present in tap water. However, nonionic surfactants are generally effective as drag reducers only in a narrow temperature range around the cloud point of the nonionic surfactant,[1] which is the temperature where the phase separation of mixture starts to occur, thus becoming cloudy. Recently, Hellsten[6,7] developed a new nonionic surfactant (SPE95285, AKZO-Nobel Chemicals)[8] as the drag-reducing additive, which consists of ethoxylated unsaturated fatty alcohols (mainly oleyl alcohol) and the other of ethoxylated unsaturated fatty acid ethanolamides, where the main component of the fatty acids is oleic acid.[3,9] The chemical structure of these two components is $R(\mathrm{OCH_2CH_2})_m\mathrm{OH}$ and $R_1\mathrm{CONH}\ (\mathrm{CH_2CH_2O})_n\mathrm{H}$. Aguilar *et al.*[10] reported that the SPE95285 surfactant was developed to operate effectively around a span of temperature between 5 and 25 °C, although it still showed drag-reduction ability up to 40 °C. Gasljevic *et al.*[9] revealed the diameter effect on the drag reduction (DR) ratio for the SPE 95285. Usui and Wakui[11] also developed a new nonionic surfactant (AROMOX, LION AKZO Co., Ltd.) as the drag-reducing additive, which mainly consisted of oleyldimethylamineoxide $[\mathrm{C_{18}H_{37}(CH_3)_2NO}=313]$ and isopropanol alcohol. Usui *et al.*[12] reported that the AROMOX surfactant had the drag-reducing ability at the wider temperature range between 10 and 40 °C.

Recently, Gurka *et al.*[13] performed particle image velocimetry (PIV) measurements on the turbulent channel flow of the nonionic surfactant Agnique KPG 264-U, which was clustered under the alkyl polyglycoside family, although the drag-reducing ability has remained unfortunately unknown. The mixture of nonionic and zwitterionic surfactants has also

a)Author to whom correspondence should be addressed. Telephone: +81 52 735 5609. Fax: +81 52 735 5247. Electronic mail: tamano.shinji@nitech.ac.jp.

been proposed as higher and more stable drag-reducing additives.[14,15] However, data on the DR of nonionic surfactants are much fewer than those of cationic surfactants.

Velocity measurements of a drag-reducing turbulent channel and pipe flows of cationic surfactant solutions have yielded valuable knowledge about the modification of turbulence statistics[16] and turbulence structures.[17,18] Quite recently, Tamano *et al.*[19] performed laser-Doppler velocimetry (LDV) and PIV measurements of the drag-reducing turbulent boundary layer in homogeneous cationic surfactant solutions at various concentrations and temperature at different streamwise locations and verified the existence of the additional maximum[20] of the streamwise turbulence intensity near the center of the boundary layer which appeared at relatively large DR ratios and small Reynolds numbers. A recent review of the DR of turbulent boundary layer due to the injection of polymer was also reported by White and Mungal.[21] However, there have been fewer studies on velocity measurements of nonionic surfactant solutions which are readily biodegraded and environmentally acceptable.

In the present study, the objective is to provide a comprehensive study on the drag-reducing ability of nonionic surfactants, i.e., the effects of the concentration and temperature of nonionic surfactant solutions on the DR obtained by measuring the pressure drop in the pipe flow and the mean velocity, turbulence statistics and structures in a zero-pressure gradient turbulent boundary layer of a homogeneous nonionic surfactant solution measured using two-component LDV and PIV systems, and to compare these results to the better studied DR by cationic surfactants.

II. NONIONIC SURFACTANT SOLUTION

The nonionic surfactant used here was AROMOX, which mainly consisted of oleyldimethylamineoxide, developed by Lion Akzo Co., Ltd.,[11] which was dissolved in tap water. The concentration of AROMOX was 50, 100, 500, and 1000 ppm by weight, and the solution temperature T was 20, 25, and 35 °C. The surfactant solutions tested were gently stirred for twelve hours in a head tank before pouring into a water tunnel. The concentration of surfactant solutions in the boundary layer and pipe flows was homogeneous.

It is known that for cationic surfactant solutions, the network structures of micelles are usually formed if the counterion, e.g., the sodium salicylate (NaSal), is mixed. On the other hand, the nonionic surfactant, oleyldimethylamineoxide, forms long threadlike micelles (the network structures) in aqueous solution without any additives.[22] This is the advantage of the nonionic surfactant, in addition to its nontoxic and biodegradable properties. Kawasaki *et al.*[23] reported the cryoTEM observation of oleyldimethylamineoxide solution which suggested that the network structures of threadlike micelles were similar to those of a cationic surfactant solution with a counterion.[24]

The shear viscosity η of the surfactant solutions tested was measured using a homemade capillary viscometer, in which the gravity flow was generated by the head tank of 1000 mm. Stainless smooth pipe with an internal diameter of $d=5.0$ mm was used. The flow rate was controlled by a needle valve and measured in terms of the weighing method. The developing region is 600 mm long ($=120d$), and the measuring region is 1400 mm long ($=280d$). A pressure transducer (GE Druck Co., Ltd., LPM5381) with a full scale of 200 Pa and linearity of ±0.25% was used for measurements of pressure loss in the measuring region. The water-jacketed structure kept solution temperature variation within ±0.5 °C during a shear viscosity measurement.

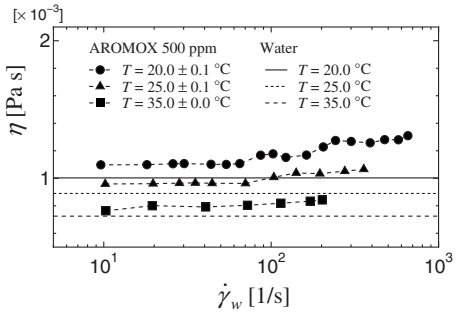

FIG. 1. Shear viscosity for AROMOX 500 ppm.

Figure 1 shows the shear viscosity η at temperature $T=20,25,35$ °C for AROMOX 500 ppm. The η is slightly larger than that of water at the same temperature, and the η is almost constant in the region of the shear rate $\dot{\gamma}_w \leq 70$ s^{-1}, and then slightly increases with the increase in the shear rate. No sudden increase in η around a critical shear rate, which was a typical indication of the shear-induced structure (SIS)[1,2] for the cationic surfactant solutions,[19] was observed. It should be noted that the constant viscosity, i.e., no sudden increase in the shear viscosity does not imply that the SIS is not formed.[3] The highest shear rate at $T=20.0$ °C corresponds to the Reynolds number of about 2000, and if the shear rate increases more, the flow becomes turbulent, to which the capillary viscometer is not applicable. Aguilar *et al.*[10] reported that the kinematic viscosity of a nonionic surfactant (SPE 95285) solution was almost independent of shear rates, but it increased with the increase in solution temperature presumably due to the formation of the SIS. These trends of SPE 95285 are similar to those of AROMOX. Therefore, it is deduced that the constant shear viscosity of AROMOX solutions is one of the fundamental properties of nonionic surfactant solutions. This rheological property of nonionic surfactants is also similar to that of polymer, which indicates that network structures of nonionic surfactant micelles are similar to those of polymer.

III. EXPERIMENTAL APPARATUS AND PROCEDURE

A. Pipe flow

Figure 2 shows the experimental setup for the measurement of the pressure drop in the pipe flow, i.e., the relation of the friction factor and the Reynolds number. The internal diameter of the pipe was $d=5.0$ mm. The pressurized flow rate was generated by the pressure tank operated at high pressure up to 0.5 MPa. The developing region is 700 mm long ($=140d$), which was longer than that of a typical drag-reducing flow ($\simeq 100d$),[3] and the measuring region is 70 mm long ($=14d$). A pressure transducer (GE Druck Co., Ltd.,

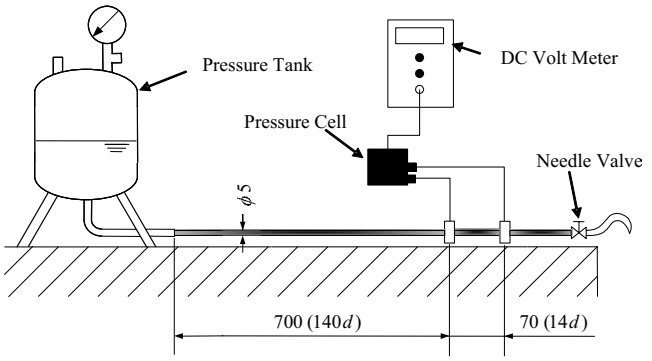

FIG. 2. Experimental apparatus for pipe flow.

LPM5481) whose full scale was 20 kPa and 100 kPa and linearity was ±0.25% was used for measurements of pressure loss. Temperature variation was within ±0.2 °C during a measurement. The flow rate was controlled by the needle valve and was measured by the weighing method.

B. Turbulent boundary layer flow on flat plate

The experiments were conducted in a closed-loop water tunnel with a cross section of 300×300 mm^2 and a length of 1500 mm in which most of a test plate of $20\times295\times1700$ mm^3 was installed, where the test plate was perpendicular to the bottom surface of the acrylic channel (see Fig. 1 in Ref. 19). All parts in contact with the surfactant solution were made of acrylic resin or stainless steel. For the LDV measurement in Sec. III, a 1-mm-diameter trip wire was fixed 100 mm downstream from the leading edge to assure a consistent transition location. The difference in free-stream velocities $U_e \simeq 300$ mm/s between the location of the leading edge of the test plate and the location 1000 mm downstream was less than 1%, where a flap was used for the zero-pressure gradient turbulent boundary layer. The working fluids, in which the solution temperature T was controlled to 25±0.1 °C by refrigerators, were circulated by a stainless steel centrifugal pump.

Figure 3 shows the present two-component LDV system with 300 mW argon-ion laser (model 1895, Kanomax Japan, Inc.), which was used in back scatter mode. The flow was seeded with nylon powder particles (mean diameter: 4.1 μm and specific gravity: 1.02). The particle concentration was about 5 ppm for the LDV measurement. LDV measurements were made 150 mm above the channel bottom, and at locations downstream from the leading edge, where $x=300$, 500, 800, or 1000 mm. The probe was slightly tilted (3°) with respect to the test plate surface in order to measure velocity very close to the wall. Although we cannot know the refractive index of AROMOX solutions which was presumably dependent on the local shear rate in the turbulent boundary layer, we assumed that the change of refractive index by the surfactant was negligible, since most of the LDV measurements agreed well with PIV measurements (as shown later in Fig. 15). Data samples in the locations away from and near the wall were about 25 000 and 10 000, respectively. The integral time of the LDV measurements was about 6 min in the region very close to the wall and about 2 min away from the wall.

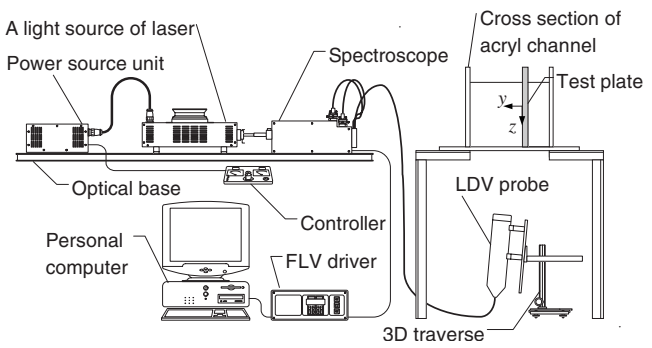

FIG. 3. Experimental apparatus for turbulent boundary layer and LDV system.

The two-dimensional PIV measurement was made for the section normal to the test plate (the streamwise and wall-normal section) which was illuminated by a laser sheet (LYPE-2SG-WL532CW, output: 1.5 W, width: 2 mm, Japan Laser, Ltd.) through the side wall of the channel, and images were captured by a high-speed camera (FASTCAM-1024PCI, Photron, Ltd.) from the bottom of the channel. The high-speed camera has a resolution of 1024×1024 pixels. The frame rate was set at 500 fps. The shutter speed was 1/5000 s. The flow was seeded with particles (Orgasol, mean diameter: 50 μm; specific gravity: 1.03). The particle concentrations for PIV measurements were about 70 and 50 ppm for water and AROMOX solutions, respectively. The interrogation region was 70×40 pixels with 57% and 75% overlap in the streamwise and wall-normal direction, respectively. The search region was 40×20 pixels. The spatial resolution of the camera was 39 μm per pixel with an effective field of view of 40×40 mm^2. PIV measurements were made for the water and the surfactant solution 1000 mm downstream from the leading edge. The turbulent statistics were obtained by evaluating 3000 images in PIV vector fields. Erroneous velocity vectors were removed, and the missing data were supplemented by interpolation of neighboring velocity vectors. The fluctuating velocity vector fields were obtained by the Reynolds decomposition.

Before starting the LDV and PIV measurements, the AROMOX solution was circulated for 16 h in order to stabilize the rheological property of solution. We confirmed that the DR ratio was almost constant after circulating AROMOX solutions for 16 h in the present water tunnel. The details of the LDV and PIV measurements were given in our previous study.[19]

IV. DRAG REDUCTION FOR PIPE FLOW

Figure 4(a) shows the relation between the friction factor λ and the Reynolds number Re for AROMOX 50, 100, 500, and 1000 ppm at $T\simeq25$ °C. In this study, the Reynolds number Re and the friction factor λ are defined as follows:

$$\mathrm{Re}=\frac{\rho U_m d}{\eta}, \tag{1}$$

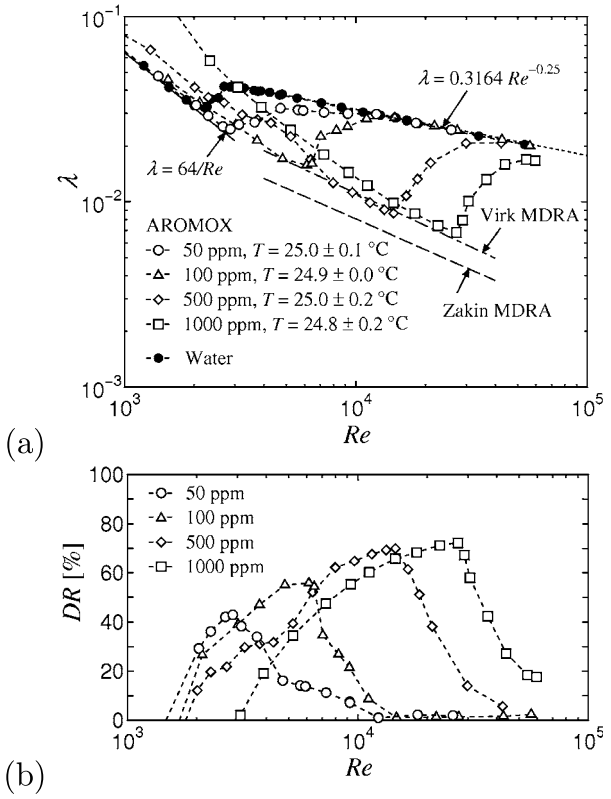

FIG. 4. Effect of solution concentration for AROMOX at $T \simeq 25$ °C: (a) λ vs Re and (b) DR vs Re.

$$\lambda = \frac{\Delta P}{\rho U_m^2/2}\frac{d}{L}, \tag{2}$$

where U_m and ρ are the bulk velocity and the density of water, respectively. To evaluate the drag-reducing ability including the variation in the shear viscosity, the values of ρ and η of water were used for nonionic surfactant solutions at the same temperature, as reported in the previous study.[1] Figure 4(a) also presents the Hagen–Poiseuille laminar theoretical relation ($\lambda = 64/\mathrm{Re}$), the Blasius turbulent empirical relation ($\lambda = 0.3164\ \mathrm{Re}^{-0.25}$) for Newtonian fluid, the Virk's maximum DR asymptote (MDRA) for polymer solutions[25] ($\lambda = 2.32\ \mathrm{Re}^{-0.58}$, $4000 < \mathrm{Re} < 40\,000$), and Zakin's MDRA for surfactant solutions[1] ($\lambda = 1.28\ \mathrm{Re}^{-0.55}$).

Figure 4(a) shows that λ for AROMOX 50, 100, and 500 ppm decreases with the increase in the Reynolds number in the region of $\mathrm{Re} \leq 2000$ and the decreasing rate is the same as that of the laminar theoretical relation. In the region of $\mathrm{Re} \leq 2000$, the values of λ for AROMOX 50, 100, and 500 ppm are larger than that of water, since the shear viscosity of water was used as the definition of the Reynolds number as described above. The friction factor is smaller at $\mathrm{Re} \geq 2000$ for AROMOX 50 and 100 ppm, at $\mathrm{Re} \geq 2500$ for AROMOX 500 ppm, and at $\mathrm{Re} \geq 3000$ for AROMOX 1000 ppm, compared with water. With the increase in the Reynolds number, λ reaches the minimum, and then approaches the Blasius relation, in which the increasing rate is almost the same as that of a cationic surfactant solution.[19] The friction factor λ for AROMOX 500 ppm is slightly smaller than Virk's MDRA, but does not reach Zakin's MDRA. It is found that the Reynolds number at the minimum of λ increases with the increase in the concentration of nonionic surfactant solution.

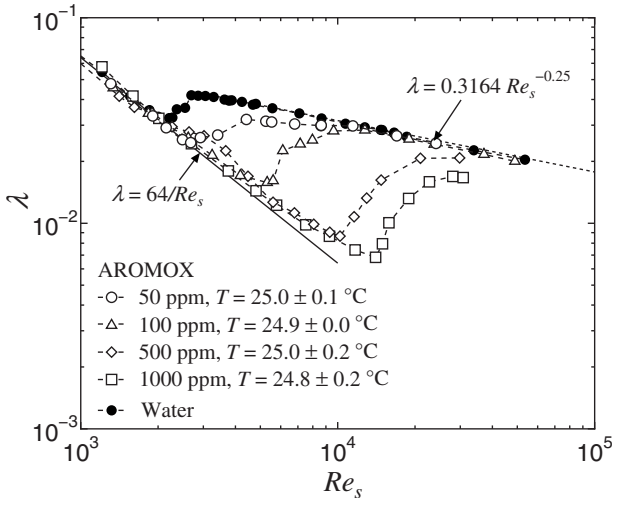

FIG. 5. Relation between friction factor λ and apparent Reynolds number based on viscosity of surfactant solutions Re_s for AROMOX at $T \simeq 25$ °C.

Figure 4(b) shows the relation between the DR ratio and Re for AROMOX 50, 100, 500, and 1000 ppm at $T \simeq 25$ °C. In the present study, the DR ratio for the pipe flow is defined as follows:

$$\mathrm{DR} = \frac{\lambda_s - \lambda}{\lambda_s} \times 100[\%], \tag{3}$$

where λ_s is the friction factor of Newtonian fluid and λ is the friction factor of nonionic surfactant solution at the same Reynolds number Re. Figure 4(b) shows that the DR increases with the increase in Re and reaches the maximum, and then decreases. This behavior is independent of the concentration of solutions. Both the maximum DR ratio and the Reynolds number at the maximum DR increase with the increase in the concentration of solutions.

Figure 5 shows the relation between friction factor λ and apparent Reynolds number Re_s for AROMOX at $T \simeq 25$ °C. Re_s is based on the viscosity η of nonionic surfactant solutions, which is obtained by the capillary viscometer. In the laminar flow region, the data on Re_s and λ agree well with the Hagen–Poiseuille laminar theoretical relation, unlike the relation between Re and λ. In the turbulent flow region, the data for the apparent Reynolds number Re_s are slightly different from those for the solvent Reynolds number Re, but the qualitative difference in the relation between λ and Re due to the definition of the Reynolds number cannot be observed, since the shear viscosity is almost independent of the shear rate.

Figure 5 also shows that measurements of λ and Re_s for all four concentrations collapse into one curve showing a smooth transition from laminar to drag-reducing turbulent flow. This behavior is typical Virk's type B DR[2] which exhibits asymptotic DR immediately after transition from laminar to turbulent flow.[9] The critical Reynolds number, at which the friction factor is minimum and the DR ratio is maximum, increases monotonically with the increase in the

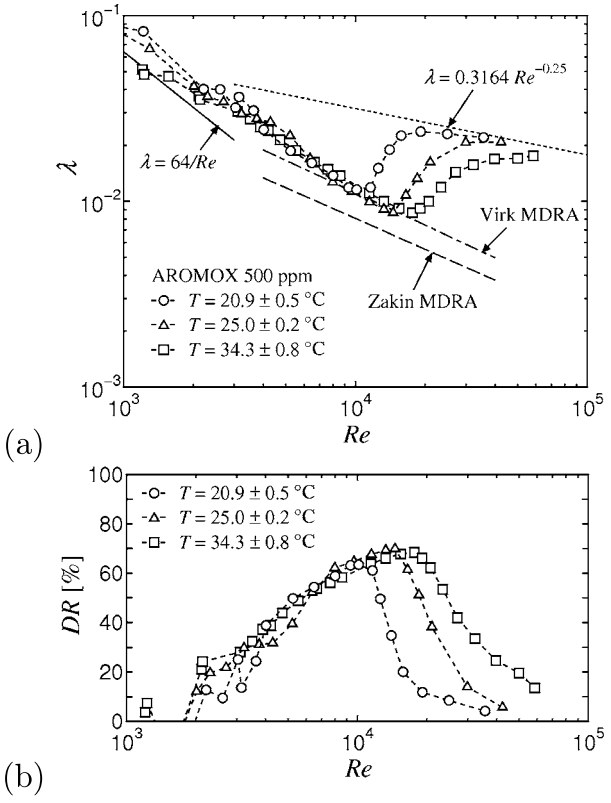

FIG. 6. Effect of solution temperature for AROMOX 500 ppm: (a) λ vs Re and (b) DR vs Re.

concentration of nonionic surfactant solution, which seems that the transition is delayed to a higher Reynolds number. In the region of Reynolds number from around 2000 to just before the critical Reynolds number, however, the flow is not laminar but drag-reducing turbulent. This is confirmed by the fact that the relation between λ and Re_s slightly deviates from the Hagen–Poiseuille laminar theoretical relation.

Figures 6(a) and 6(b) show the relation between λ and Re and the relation between DR and Re at $T \simeq 20$, 25, and 35 °C for AROMOX 500 ppm, respectively. At $Re < 2500$, the λ of the AROMOX solution at $T \simeq 20$, 25, and 35 °C is larger than that of the laminar theoretical relation and the decreasing rate of λ versus Re is the same as that of the laminar relation. In the region of $2500 \leq Re \leq 10\,000$, the relations between λ and Re agree well with one another, and the value of λ is smaller than that of water, which indicates the friction drag is reduced. The DR increases with the increase in Re and the maximum DR up to 70% can be obtained, which seems to be independent of the solution temperature. The Reynolds number at the maximum DR slightly increases with the increase in solution temperature.

It is known that the friction factor, i.e., DR level as a function of the Reynolds number for pipe flows depends on the diameter in addition to the concentration and temperature of surfactant solutions, while the critical wall-shear stress is independent of the diameter for the surfactant solution.[1,2] Gasljevic *et al.*[9] clarify that data on the DR level as a function of bulk velocity for various pipe diameters are very well correlated by a single curve for a cationic surfactant Ethoquad solution, while scaling DR with bulk velocity does not

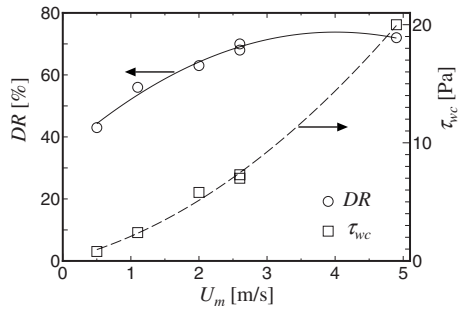

FIG. 7. DR ratio and critical wall-shear stress as a function of bulk velocity for the data shown in Figs. 4 and 6.

work satisfactorily for the nonionic surfactant SPE95285 solution. They also found that the data on SPE95285 solutions for various pipe diameters well correlated by a straight line, when the data were plotted as wall-shear stress versus bulk velocity. Figure 7 shows the DR ratio and critical wall-shear stress τ_{wc} as a function of bulk velocity U_m for the data in Figs. 4 and 6. Data on DR versus U_m and τ_{wc} versus U_m are well scaled by single curves, respectively. Unfortunately, data in Fig. 7 are presented for one single diameter. For discussion of the size effect of AROMOX solutions, measurements with various pipe diameters would be required.

We performed the pressure drop measurements of pipe flow in used nonionic solutions several times, and confirmed that the relation between λ and Re was not changed (not shown here). This indicates that the degradation due to the shear of the pipe flow is negligible. There is also the concern that the drag-reducing ability becomes weaker or disappears with the long time elapsed, since the nonionic surfactant solution has biodegradable properties. The AROMOX solution used here is completely biodegradable for about one month under the activated sludge condition, according to reference data of Lion Akzo Co., Ltd. Figure 8 shows the effect of elapsed time on the relation between λ and Re at $T \simeq 25$ °C for AROMOX 500 ppm. The nonionic surfactant solution was stored in a tank at room temperature with sun-

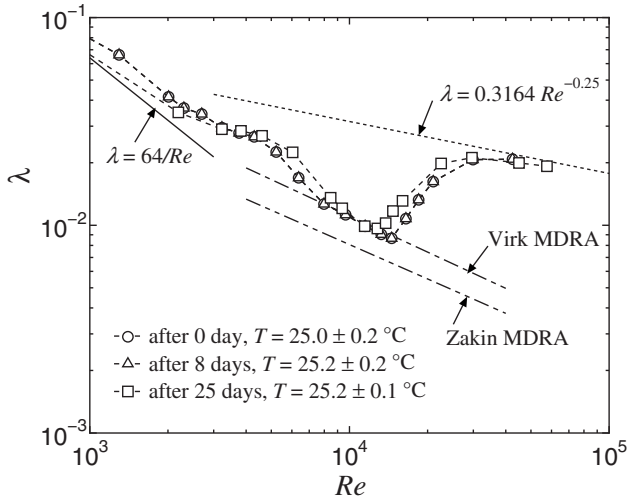

FIG. 8. Effect of elapsed time on relation between λ and Re for AROMOX 500 ppm at $T \simeq 25$ °C.

TABLE I. Boundary layer parameters and friction velocity at $T=25$ °C for AROMOX 500 ppm and water.

	x (mm)	δ (mm)	δ^* (mm)	θ (mm)	u_τ (mm/s)
AROMOX 500 ppm	300	13.5	2.27	1.56	16.6
	500	16.7	2.88	1.94	14.2
	800	22.8	3.89	2.52	11.6
	1000	26.1	4.34	2.74	10.3
Water	300	13.6	2.38	1.60	15.4
	500	19.2	3.28	2.26	14.7
	800	24.3	4.17	2.89	14.1
	1000	28.9	5.13	3.56	13.6

light shut out. It is confirmed that the difference in the relation between λ and Re due to the elapsed time cannot be observed. It can be concluded that the biodegradable property of AROMOX solution used does not invalidate the present experimental results.

The present pressure drop measurements for pipe flow of nonionic surfactant (AROMOX) solutions indicated that the DR ratio decreases sharply with increasing the Reynolds number after reaching the maximum DR ratio, which is consistent with previous study of nonionic surfactants (AROMOX and SPE95258).[3,12] This behavior is similar to that of cationic surfactant solutions but not similar to that of polymer solutions, in which the decrease in DR with increasing Re is not observed.[2] Gasljevic *et al.*[3] claimed that for the nonionic SPE95258 surfactant, the total degradation, which seemed to imply degradation of micelles themselves, was observed beyond a critical wall-shear stress, and only the SIS was destroyed at some lower level of the wall-shear stress. Regarding the present measurements, it is deduced that only network structures of nonionic surfactant micelles are destroyed in the region of decrease in DR. Moreover, even in the zero DR region at the higher Re, the micelles are not destroyed completely, since the DR can be obtained for used nonionic surfactant solutions repeatedly. The broken and reformed property seems to be common to both nonionic and cationic surfactants, and it is one of the largest differences from a covalently bonded polymer backbone.

V. LDV MEASUREMENTS FOR BOUNDARY LAYER FLOW ON FLAT PLATE

A. Boundary layer parameters and drag reduction ratio

Table I shows a comprehensive listing of boundary layer parameters such as boundary layer thickness δ, displacement thickness δ^*, momentum thickness θ, and the friction velocity u_τ at $x=300$, 500, 800, and 1000 mm for AROMOX 500 ppm and water at $T=25$ °C. The friction velocity u_τ was obtained by estimating the wall-shear stress from the mean velocity gradient and the shear viscosity at the wall for AROMOX solution, and by the Clauser method for water. Table I shows that the length scales δ, δ^*, and θ for AROMOX 500 ppm increase in the streamwise direction, and both their values and their developing rate are smaller than those of water. Except at $x=300$ mm, the u_τ for the surfactant solutions is smaller than that for water at the same x, which indicates the DR. Note that the DR ratio is evaluated at the same Re as described later.

Figures 9(a) and 9(b) show the dependence of the friction coefficient $C_f=2(u_\tau/U_e)^2$ and the shape factor $H=\delta^*/\theta$ on the momentum-thickness Reynolds number Re_θ, respectively. The Reynolds number Re_θ is defined as follows:

$$\mathrm{Re}_\theta=\frac{U_e\theta}{\nu}, \tag{4}$$

where ν is the kinematic viscosity and is determined using the shear rate at the wall for AROMOX 500 ppm. In the figure, the solid and dotted lines represent Coles' curve[26] and Blasius laminar line,[27] respectively. Figure 9(a) shows that C_f for AROMOX monotonically decreases with the increase

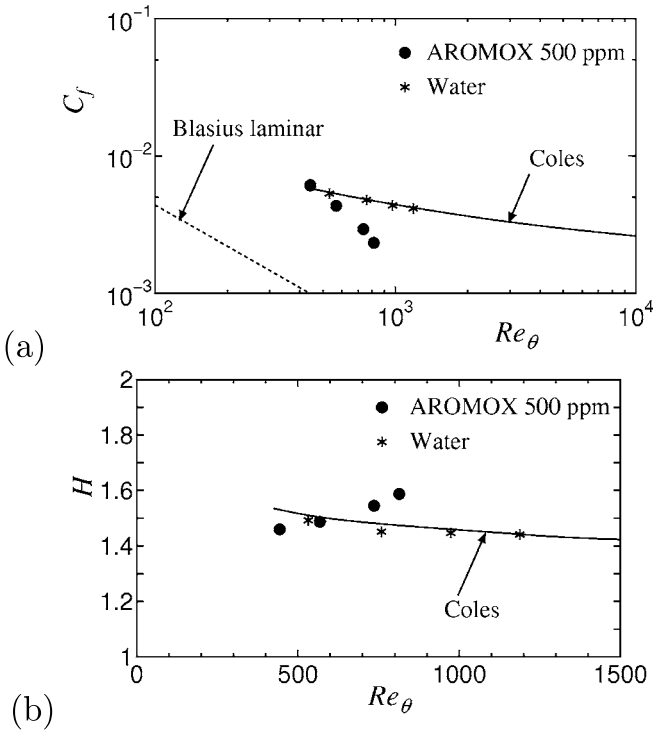

FIG. 9. Streamwise evolution of boundary layer: (a) friction coefficient and (b) shape factor.

TABLE II. DR ratio (%) in the turbulent boundary layer at $T=25$ °C for AROMOX 500 ppm.

x (mm)	300	500	800	1000
DR (%)	−5	18	40	50

in Re_θ, in which the slope is larger than that of the Blasius laminar line. Figure 9(b) shows the value of H slightly increases with the increase in Re_θ, whereas it decreases for water, whose variation is the same as that of cationic surfactant solution.[19]

In the present study, the DR ratio for the turbulent boundary layer is defined as follows:

$$\mathrm{DR} = \frac{C_{f,\mathrm{water}} - C_{f,\mathrm{surfactant}}}{C_{f,\mathrm{water}}} \times 100, \tag{5}$$

under the condition of the same momentum-thickness Reynolds number Re_θ. The C_f for water is obtained using the Coles' curve at the corresponding Reynolds number. Therefore, the error for DR is caused by the friction factor for surfactant solution. The wall-shear stress was obtained by the mean velocity gradient which was obtained by the least square approximation using mean velocity measurements (three to five points) at different y locations within the viscous sublayer ($y^+<5$). In case of drag-reducing surfactant solutions, a dimensional length of the viscous sublayer becomes larger with the increase in DR. Therefore, we can obtain the mean velocity gradient near the wall for surfactant solutions more accurately, compared with Newtonian flow. We confirmed that the error bar of DR of ±5% was estimated by several velocity measurements near the wall. Table II shows the DR at $x=300$, 500, 800, 1000 mm, and $T=25$ °C for AROMOX 500 ppm. The DR becomes larger downstream from $x=300$ to 1000 mm. In the present study, the maximum DR ratio is DR=50% at $x=1000$ mm. The wall-shear stress, $\tau_w=\rho u_\tau^2$, for the turbulent boundary layer flow in AROMOX 500 ppm is 0.1 Pa at $x=1000$ mm, which is within the wall-shear stress τ_w obtained for the pipe flow with the positive DR but much smaller than the critical wall-shear stress τ_{wc}.

B. Mean velocity

The distributions of mean velocities scaled by the free-stream velocity and the friction velocity U/U_e and $U^+=U/u_\tau$ are shown in Figs. 10(a) and 10(b), respectively. The abscissae y/δ and $y^+=u_\tau y/\nu$ are the distance from the wall scaled by the boundary layer thickness δ and the viscous length scale, respectively. The measurement locations are $x=300$, 500, 800, and 1000 mm for surfactant solutions, and $x=500$ and 1000 mm for water. In Fig. 7(a), the solid and dotted lines in the figure represent $1/n$th-power law ($n=6$) and the Blasius laminar profile,[27] respectively. In Fig. 10(b), the linear profile $U^+=y^+$, the log-law profile ($U^+=2.44\ln y^+ +5.0$), and Virk's ultimate profile[25] ($U^+=11.7\ln y^+ -17$) are also shown.

The mean velocities U/U_e at $x=300$ and 500 mm (DR=−5% and 18%) are collapsed on that of water across the boundary layer. The mean velocity U/U_e at $x=800$ and 1000 mm (DR=40% and 50%) are similar to each other, and they are slightly smaller than that for water near the wall ($y/\delta<0.2$). It is noticeable that the profile of U/U_e approaches the Blasius laminar profile with the increase in DR for the cationic surfactant solution,[19] while no such tendency can be observed for the nonionic surfactant solution.

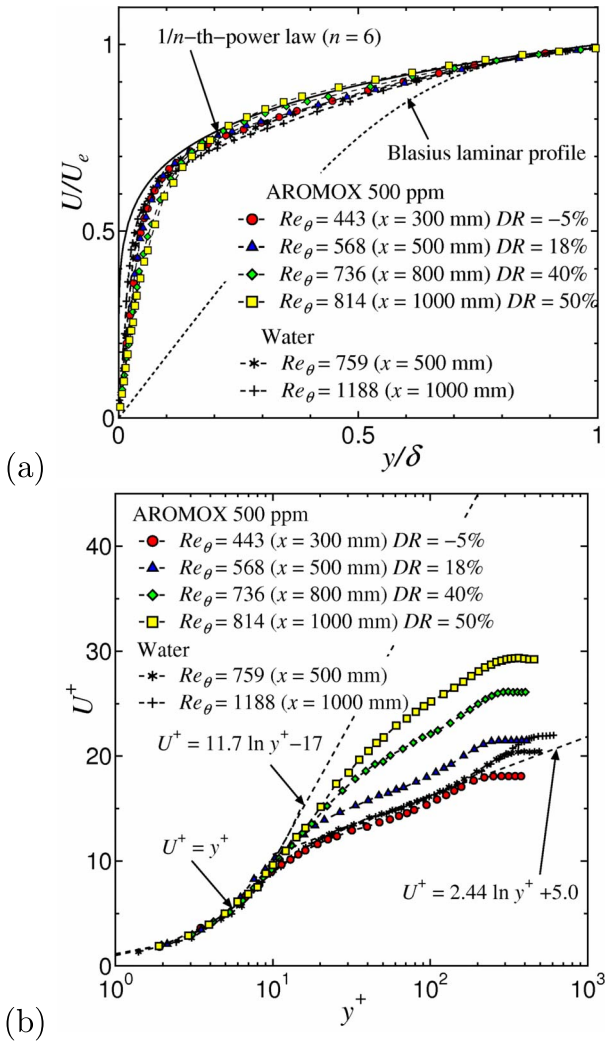

FIG. 10. (Color online) Mean velocity profiles for AROMOX 500 ppm: (a) with outer scaling and (b) in wall coordinates.

Compared with water, the profiles of U^+ at DR=−5% and 18% shift downward and upward in the logarithmic region, respectively, but their slope is almost the same as that for water. With the increase in DR from 18% to 50%, the value of U^+ at $y^+>10$ increases, and the slope of U^+ becomes slightly larger. The same tendency has also been reported in the previous study of the turbulent boundary layer in the cationic surfactant solution.[19]

C. Turbulence statistics

Figure 11 shows the distribution of streamwise turbulence intensity scaled by friction velocity $u'^+_{\mathrm{rms}}=u'_{\mathrm{rms}}/u_\tau$. The peak values of u'^+_{rms} for $DR=40\%$ and 50% were larger than that for water, which is supported by numerous previous studies.[19] According to our earlier study[19] at various Rey-

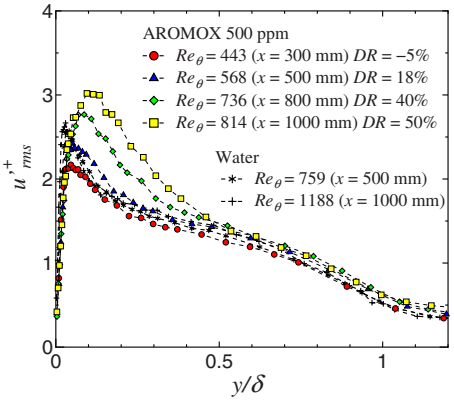

FIG. 11. (Color online) Streamwise turbulence intensity for AROMOX 500 ppm.

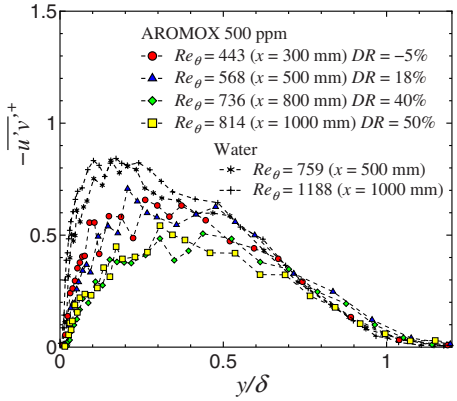

FIG. 13. (Color online) Reynolds shear stress for AROMOX 500 ppm.

nolds numbers under different concentrations and temperatures for the turbulent boundary layer in cationic surfactant solution, however, the near-wall maximum is not related to the DR ratio directly. White and Mungal[21] also pointed out that the development process of the boundary layer is complex owing to the history effect of the polymer-turbulence interaction. Thus, further investigations would be needed to conclude the relation between the maximum of u'^+_{rms} and DR. For DR=40% and 50%, the value of y/δ at the maximum of u'^+_{rms} for surfactant solutions seems to be larger than that for water, as reported in the literature.[19]

Tamano *et al.*[19] verified the existence of the additional maximum of the streamwise turbulence intensity near the center of the boundary layer in various experimental conditions and proposed the bilayered structure model, which is assumed so that the formation of the SIS in the turbulent flow of the dilute cationic surfactant solution is strongly related to the viscoelasticity and the DR. In the present study on nonionic surfactant (AROMOX) solutions, the additional maximum of u'^+_{rms} cannot be observed. This could be explained by the fact that the sudden increase in the shear viscosity is not observed for nonionic surfactant solutions (see Fig. 2).

Figure 12 shows the distribution of wall-normal turbulence intensity scaled by friction velocity v'^+_{rms}. As decreasing DR, the v'^+_{rms} decreases in the region from the wall to around the center of the boundary layer. Although the v'^+_{rms} for the cationic surfactant solution is much smaller than that for water and is virtually constant across the boundary layer,[19] such a tendency is not observed for AROMOX 500 ppm. The maximum of v'^+_{rms} at x=300 mm (DR=−5% and Re_θ=443) is smaller than that of water, which may be due to the effect of small Reynolds number.

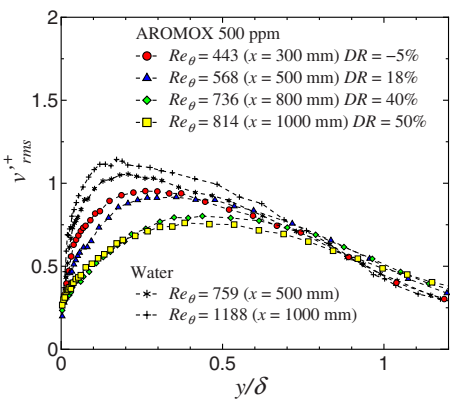

FIG. 12. (Color online) Wall-normal turbulence intensity for AROMOX 500 ppm.

Figure 13 shows the distribution of Reynolds shear stress scaled by the friction velocity $-\overline{u'v'}^+$. The Reynolds shear stress for AROMOX 500 ppm becomes smaller with the increase in DR. It has been reported that the Reynolds shear stress was almost zero at the large DR ratio for the drag-reducing turbulent boundary layer in the cationic surfactant solution.[19] Even at DR=50%, however, the maximum of the Reynolds shear stress for AROMOX 500 ppm is almost half that of water. This may be due to the difference in the Reynolds number and the concentration and temperature of solutions, in addition to the difference in the type of surfactant. Such investigation is beyond the scope of the present work.

It was found that as a whole, turbulence statistics for nonionic AROMOX solutions were similar to those for polymer solutions, rather than cationic solutions.[2]

D. Shear stress profiles

The total shear stress is the sum of viscous shear stress dU^+/dy^+, turbulent shear $-\overline{u'v'}^+$, and polymer stress or surfactant micellar stress τ_p.[16] It is considerably difficult to measure the polymer stress τ_p directly and accurately. Therefore, if the total shear stress can be obtained, the polymer stress can be obtained. We cannot assume a nominally constant shear stress region near the wall for turbulent boundary layers of viscoelastic fluids, unlike Newtonian fluids. It is also difficult, however, to obtain the total shear stress for the turbulent boundary layer, unlike the turbulent channel flow, in which the total shear stress or the wall-shear stress is determined by the force balance with the pressure drop.[16] Recently, Hou *et al.*[28] proposed a new technique to determine total shear stress in a turbulent boundary layer with polymer additives. Their method is based on the $(1-y/\delta)$ weighted straight-line fit.

Figures 14(a) and 14(b) show profiles of $dU^+/dy^+ - \overline{u'v'}^+$ and $(1-y/\delta)$ $(dU^+/dy^+ - \overline{u'v'}^+)$ for AROMOX

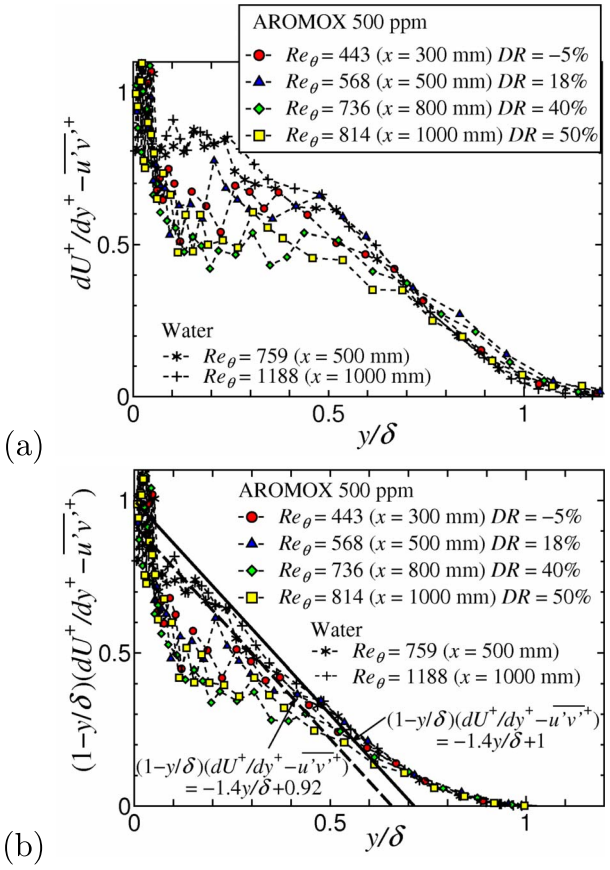

FIG. 14. (Color online) Profiles of $dU^+/dy^+ - \overline{u'v'}^+$ for AROMOX 500 ppm: (a) $dU^+/dy^+ - \overline{u'v'}^+$ and (b) $(1-y/\delta)\ (dU^+/dy^+ - \overline{u'v'}^+)$.

500 ppm, respectively. In Fig. 14(b), the solid line represents the relation for Newtonian fluid at relatively low Reynolds numbers, $(1-y/\delta)\ (dU^+/dy^+ - \overline{u'v'}^+) = -1.4y/\delta + 1$. To clarify the deviation of data on water from the $(1-y/\delta)$ fit, the relation, $(1-y/\delta)\ (dU^+/dy^+ - \overline{u'v'}^+) = -1.4y/\delta + 0.92$, is also presented as a dashed line. It is found that the $(1-y/\delta)$ fit is reasonable for water at $x=1000$ mm, while the quality of LDV data on water at $x=500$ mm is relatively low. Hou *et al.*[28] clarified the possible dependencies of the $(1-y/\delta)$ fit parameters, (a,b) of $(1-y/\delta)\ (dU^+/dy^+ - \overline{u'v'}^+) = -ay/\delta + b$, and showed that the slope $-a$ might be related to whether the turbulent boundary layer was fully developed or not, while the intercept b was almost unity and constant in the region of low Reynolds numbers. In the present study for water, $-a$ is almost independent of Re_θ, and $b(=0.92)$ at $x=500$ mm is smaller than unity, which is not consistent with the finding of Hou *et al.*[28] The reason still remains unknown.

The shear stress $dU^+/dy^+ - \overline{u'v'}^+$ for AROMOX 500 ppm is smaller than that of water in the region $0.1 < y/\delta < 0.4$. The weighted shear stress $(1-y/\delta)\ (dU^+/dy^+ - \overline{u'v'}^+)$ for AROMOX 500 ppm seems to be more collapsed compared with the nonweighted case, but the value is still smaller than that of water. This is different from the finding of Hou *et al.*[28] in which the values of $(1-y/\delta)\ (dU^+/dy^+ - \overline{u'v'}^+)$ for polymer solution agree well with those for water in the region $0.2 < y/\delta < 0.5$. This discrepancy is due to the difference between the turbulent boundary layers with the polymer additive and in homogeneous surfactant solutions. The method of Hou *et al.*[28] presumes that the polymer stress is significant near the wall and negligible away from it.

VI. PIV MEASUREMENTS FOR BOUNDARY LAYER FLOW ON FLAT PLATE

A. Statistics

To show the accuracy of the present PIV measurements for both water and AROMOX 500 ppm with DR=50% via the LDV measurement, the mean velocity U/U_e, streamwise and wall-normal turbulence intensities u'_{rms}/U_e and v'_{rms}/U_e, and Reynolds shear stress $-\overline{u'v'}/U_e^2$ at $x=1000$ mm and $T=25\ ^\circ\mathrm{C}$ were compared to the corresponding data obtained by the LDV measurement in Fig. 15. Figures 15(a), 15(b), and 15(d) show that the profiles of mean velocity, streamwise turbulence intensity, and Reynolds shear stress for both the water and surfactant solution obtained by the PIV measurement agree well with the corresponding data obtained by the LDV measurement. Figure 15(c) shows that the wall-normal turbulence intensity for the PIV measurement is somewhat smaller than that for the LDV measurement, which is due to the lack of spatial resolution of the PIV measurement.[19,29] Therefore, it can be concluded that the velocity fields obtained by the present PIV measurements are reliable for the discussion of turbulence structures.

B. Fluctuating velocity vector fields

Figure 16 shows the time sequence realization of typical fluctuating velocity vector fields in streamwise and wall-normal $(x\text{-}y)$ plane for the water. Flow is from left to right. In the figure, x' represents the left end of the image obtained and $y=0$ is the location of the wall. The vector represents the fluctuating velocity vector. In Fig. 16(a), we can observe the sweep event (A) and two vortex cores (B and C) which seem to constitute a hairpin vortex packet. Subsequently, the vortex core (D) appears in Fig. 16(b). After that, the ejection appears in the region of the whole boundary layer (not shown here). This kind of process observed for water is consistent with a self-sustaining mechanism of near-wall turbulence.[30,31]

Figures 17(a) and 17(b) show the time sequence of fluctuating velocity vector fields for AROMOX 500 ppm with $DR=50\%$. The arrow scale is the same as that for water. In Fig. 17(a), the velocity fluctuations are attenuated across the turbulent boundary layer, and only one vortex (E), the scale of which is larger than that of water, is observed. Distinct sweep and ejection events are not observed. Figure 17(b) shows that in the region (F), the fluctuating velocity vectors are almost parallel to the wall, and the velocity vectors are in the negative direction. In our previous study of cationic surfactant solutions,[19] the same trend of fluctuating velocity vector in the region (F) has been observed. In the present study, however, we cannot find the bilayered structure,[19] which is the typical structure for the cationic surfactant solutions at relatively high DR ratio and results in the additional maximum of the streamwise turbulence intensity. This

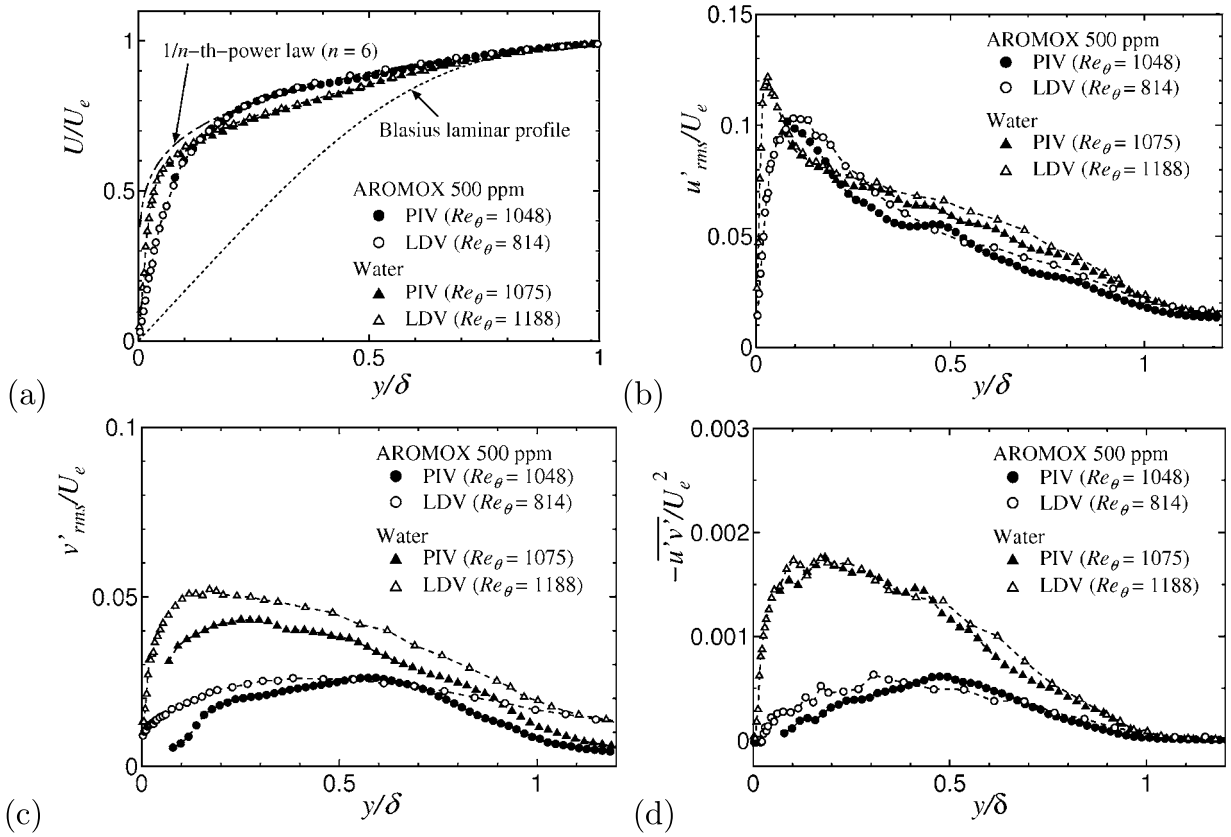

FIG. 15. Comparison of statistics between PIV and LDV at $x=1000$ mm, $T=25$ °C for water and AROMOX 500 ppm with $DR=50\%$: (a) mean velocity, (b) streamwise turbulence intensity, (c) wall-normal turbulence intensity, (d) and Reynolds shear stress.

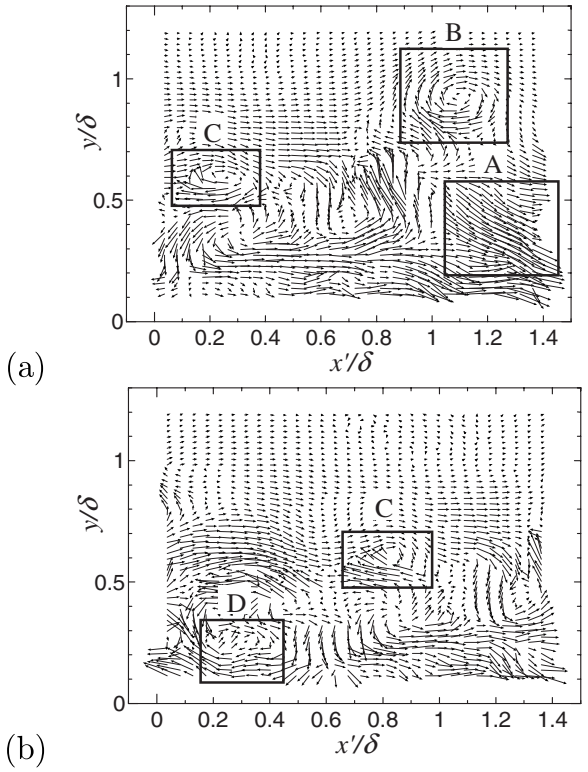

FIG. 16. Fluctuating velocity vector fields in x-y plane for water: (a) $t=t_1$ s and (b) $t=t_1+0.06$ s.

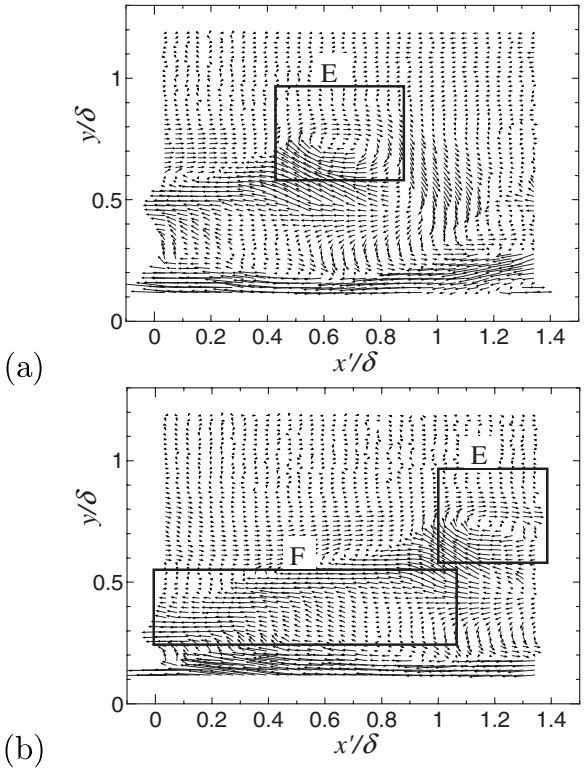

FIG. 17. Fluctuating velocity vector fields in x-y plane for AROMOX 500 ppm: (a) $t=t_2$ s and (b) $t=t_2+0.06$ s.

difference is due to the fact that the sudden increase in the shear viscosity is observed for the cationic surfactant solution and not observed for the nonionic surfactant solution, as mentioned in Sec. V C.

VII. CONCLUSION AND DISCUSSION

In the present study, the drag-reducing effect of nonionic surfactant solutions which were nontoxic and biodegradable was investigated for the pipe flow and turbulent boundary layer. As the nonionic surfactant solution, AROMOX which mainly consisted of oleyldimethylamineoxide was used. The measurement of the pressure drop in the pipe flow with the internal diameter of $d=5.0$ mm at solvent Reynolds numbers Re between 1000 and 60 000 revealed the effects of the concentration and temperature of AROMOX solutions on the DR. The drag-reducing effect of a nonionic surfactant on the turbulent boundary layer at momentum-thickness Reynolds numbers Re_θ from 443 to 814 was also investigated using a two-component LDV system. The DR ratio increases with the increase in the Reynolds number until it approaches maximum, and then the ratio rapidly decreases with the increase in Reynolds number, whose trend is similar to that of cationic surfactant solutions. It was found that at the temperature of nonionic surfactant solutions $T=25\ ^\circ\mathrm{C}$, the maximum DR ratio for AROMOX 500 ppm was about 50%, in the boundary layer flow, although the DR ratio was larger than 60% in pipe flow.

Turbulence statistics for AROMOX 500 ppm showed the behavior of typical drag-reducing flow such as the shift up in the log-law region for the mean velocity in wall-units, the increase in the maximum of the streamwise turbulence intensity, and the decrease in the wall-normal turbulence intensity. The maximum of the Reynolds shear stress for AROMOX 500 ppm was almost half that of water, and not close to the zero value, unlike the cationic surfactant solution. It was revealed that turbulence statistics for turbulent boundary layers of nonionic AROMOX solutions were similar to those for polymer solutions, rather than cationic solutions, while the relation between the DR and Reynolds number for pipe flows of nonionic AROMOX solutions was similar to that for cationic solutions, rather than polymer solutions. This may be attributed to the difference in SIS formations between nonionic and cationic surfactant solutions, and the difference in the durability for shear stress between network structures of polymer and nonionic surfactant micelles.

In addition, the PIV measurements revealed that turbulence structures for AROMOX 500 ppm were suppressed and modified, which was consistent with the previous studies on the turbulent boundary layer with polymer additives.[21] In the present study of nonionic surfactant solution with the non-SIS property, however, we could not see the bilayered structure,[19] which was the typical structure for the cationic surfactant solutions with the SIS property. As the present investigation of the turbulent statistics and structures in the drag-reducing turbulent boundary layer of nonionic surfactant solutions was a first attempt, further experimental investigation using the LDV and PIV measurements under various concentration and temperature of nonionic surfactant solutions would be warranted for further discussion of possible differences in turbulence statistics and structures between nonionic and cationic surfactant solutions or between nonionic and polymer solutions.

ACKNOWLEDGMENTS

This work was partially supported by a Grant-in-Aid for Scientific Research (Grant Nos. 19560170 and 21760126) from the Japan Society for the Promotion of Science. The authors wish to thank J. Suzuki for his unfailing assistance with the experimental measurements. Special thanks are also due Lion Akzo Co., Ltd. for providing the nonionic surfactant solutions.

[1] J. L. Zakin, B. Lu, and H.-W. Bewersdorff, "Surfactant drag reduction," Rev. Chem. Eng. **14**, 253 (1998).
[2] A. Gyr and H.-W. Bewersdorff, *Drag Reduction of Turbulent Flows by Additives* (Kluwer, Dordrecht, 1995).
[3] K. Gasljevic, K. Hoyer, and E. F. Matthys, "Temporary degradation and recovery of drag-reducing surfactant solutions," J. Rheol. **51**, 645 (2007).
[4] J. L. Zakin and J. L. Chiang, "Non-ionic surfactants as drag reducing additives," Nature (London) Phys. Sci **239**, 26 (1972).
[5] J. L. Zakin and H.-L. Lui, "Variables affecting drag reduction by nonionic surfactant additives," Chem. Eng. Commun. **23**, 77 (1983).
[6] I. Harwigsson and M. Hellsten, "Environmentally acceptable drag-reducing surfactants for district heating and cooling," J. Am. Oil Chem. Soc. **73**, 921 (1996).
[7] M. Hellsten, "Drag-reducing surfactants," J. Surfactants Deteg. **5**, 65 (2002).
[8] M. Hellsten and I. Harwigsson, U.S. Patent No. 5,339,855 (1994).
[9] K. Gasljevic, G. Aguilar, and E. F. Matthys, "On two distinct types of drag-reducing fluids, diameter scaling, and turbulent profiles," J. Non-Newtonian Fluid Mech. **96**, 405 (2001).
[10] G. Aguilar, K. Gasljevic, and E. F. Matthys, "Asymptotes of maximum friction and heat transfer reductions for drag-reducing surfactant solutions," Int. J. Heat Mass Transfer **44**, 2835 (2001).
[11] H. Usui and F. Wakui, Japanese Patent Nos. H9-302324 and H9-302375 (1997).
[12] H. Usui, H. Kariyama, T. Saeki, H. Sugawara, and F. Wakui, "Effect of surfactant molecular structure on turbulent drag reduction," Kagaku Kogaku Ronbunshu **24**, 134 (1998) (in Japanese).
[13] R. Gurka, A. Liberzon, and G. Hetsroni, "Characterization of turbulent flow in a flume with surfactant," J. Fluids Eng. **126**, 1054 (2004).
[14] W. A. Aly, H. Inaba, N. Haruki, and A. Horibe, "Drag and heat transfer reduction phenomena of drag-reducing surfactant solutions in straight and helical pipes," J. Heat Transfer **128**, 800 (2006).
[15] S.-H. Cho, C.-S. Tae, and M. Zaheeruddin, "Effect of fluid velocity, temperature, and concentration of non-ionic surfactants on drag reduction," Energy Convers. Manage. **48**, 913 (2007).
[16] M. D. Warholic, G. M. Schmidt, and T. J. Hanratty, "The influence of a drag-reducing surfactant on a turbulent velocity field," J. Fluid Mech. **388**, 1 (1999).
[17] Y. Kawaguchi, T. Segawa, Z. Feng, and P. Li, "Experimental study on drag-reducing channel flow with surfactant additives–spatial structure of turbulence investigated by PIV system," Int. J. Heat Fluid Flow **23**, 700 (2002).
[18] F.-C. Li, Y. Kawaguchi, B. Yu, J.-J. Wei, and K. Hishida, "Experimental study of drag reduction mechanism for a dilute surfactant solution flow," Int. J. Heat Mass Transfer **51**, 835 (2008).
[19] S. Tamano, M. Itoh, T. Inoue, K. Kato, and K. Yokota, "Turbulence statistics and structures of drag-reducing turbulent boundary layer in homogenous aqueous surfactant solutions," Phys. Fluids **21**, 045101 (2009).
[20] M. Itoh, S. Tamano, K. Yokota, and M. Ninagawa, "Velocity measurement in turbulent boundary layer of drag-reducing surfactant solution," Phys. Fluids **17**, 075107 (2005).

[21]C. M. White and M. G. Mungal, "Mechanics and prediction of turbulent drag reduction with polymer additives," Annu. Rev. Fluid Mech. **40**, 235 (2008).
[22]T. Shikata, M. Shiokawa, S. Itatani, and S. Imai, "Viscoelastic behavior of aqueous surfactant micellar solutions," Korea-Aust. Rheol. J. **14**, 129 (2002).
[23]H. Kawasaki, M. Souda, S. Tanaka, N. Nemoto, G. Karlsson, M. Almgren, and H. Maeda, "Reversible vesicle formation by changing pH," J. Phys. Chem. B **106**, 1524 (2002).
[24]B. Lu, X. Li, L. E. Scriven, H. T. Davis, Y. Talmon, and J. L. Zakin, "Effect of chemical structure on viscoelasticity and extensional viscosity of drag-reducing cationic surfactant solutions," Langmuir **14**, 8 (1998).
[25]P. S. Virk, "Drag reduction fundamentals," AIChE J. **21**, 625 (1975).
[26]D. E. Coles, "A manual of experimental boundary-layer practice for low-speed flow," RAND Report No. R-403-PR, 1962.
[27]H. Schlichting, *Boundary-Layer Theory*, 7th ed. (McGraw-Hill, New York, 1979).
[28]Y. Hou, V. S. R. Somandepalli, and M. G. Mungal, "A technique to determine total shear stress and polymer stress profiles in drag reduced boundary layer flows," Exp. Fluids **40**, 589 (2006).
[29]M. D. Warholic, D. K. Heist, M. Katcher, and T. J. Hanratty, "A study with particle-image velocimetry of the influence of drag-reducing polymers on the structure of turbulence," Exp. Fluids **31**, 474 (2001).
[30]R. J. Adrian, "Hairpin vortex organization in wall turbulence," Phys. Fluids **19**, 041301 (2007).
[31]S. K. Robinson, "Coherent motions in the turbulent boundary layer," Annu. Rev. Fluid Mech. **23**, 601 (1991).